Journal of
Materials Chemistry A

This article can be cited before page numbers have been issued, to do this please use: P. Pachfule, X. Yang, Q. Zhu, N. Tsumori, T. Uchida and Q. Xu, *J. Mater. Chem. A*, 2017, DOI: 10.1039/C6TA10748F.

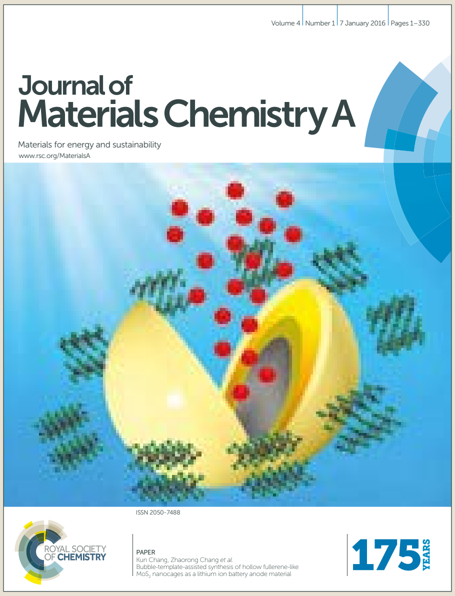

rsc.li/materials-a

Journal of
Materials Chemistry A

View Article Online
DOI: 10.1039/C6TA10748F

PAPER

From Ru nanoparticle-encapsulated metal-organic framework to highly catalytically active Cu/Ru nanoparticle-embedded porous carbon

Received 00th January 20xx,
Accepted 00th January 20xx

DOI: 10.1039/x0xx00000x

www.rsc.org/

Pradip Pachfule,[a] Xinchun Yang,[a,b] Qi-Long Zhu,[a] Nobuko Tsumori,[c] Takeyuki Uchida,[a] and Qiang Xu*[a,b]

A facile method for in situ encapsulation of highly dispersed ultrafine Ru nanoparticles in HKUST-1, a copper–1,3,5-benzenetricarboxylate (BTC) metal-organic framework (MOF), without aggregation on the external surface of MOF crystallites has been developed. The thermal transformation of Ru@HKUST-1 composites in an inert atmosphere has yielded the ultrafine Cu/Ru nanoparticle-embedded porous carbon, which show very high catalytic activity and good durability for ammonia borane hydrolysis. During the thermal treatment of Ru@HKUST-1 composites, highly graphitic carbon formed around the Cu/Ru nanoparticles depressed the sintering of nanoparticles, resulting in the fine distribution of tiny nanoparticles in carbon matrix. For the first time, the utilization of metal nanoparticle-encapsulated MOFs as a template/precursor for the synthesis of catalytically active metal nanoparticle-embedded porous carbon has been revealed.

Introduction

The Heterogeneous catalysis based on metal nanoparticle catalysts is of paramount importance in many areas of the chemical and energy industries due to their uncountable applications.[1,2] Supported monometallic and bimetallic nanoparticles have been extensively applied as heterogeneous catalysts, while they often suffer from particle aggregation during the reaction process and thus a corresponding loss of catalytic activity. So far, extensive efforts have been devoted for resolving the stability issues of supported metal nanocatalysts.[3,4] Metal–organic frameworks (MOFs)[5,6] have been used as supports for effectively immobilizing metal nanoparticles inside pores by the nano-confinement effects,[7-9] while most of the MOFs have limited thermal and chemical stabilities. Therefore, it is highly desired to develop a methodology to effectively immobilize metal nanoparticles with controlled growth and high stability on stable supports. Herein, we have developed a novel strategy for the synthesis of highly dispersed Cu/Ru nanoparticle-embedded porous carbon composites using the Ru nanoparticle-encapsulated Cu-MOF composites, which have been synthesized by a facile one-pot in situ method, as a self-dedicated template/precursor (Fig. 1). The small sized Cu/Ru nanoparticle-embedded porous carbon materials exhibit significant catalytic activity, and in particular, excellent durability for hydrolysis of ammonia borane (AB).[10,11]

The synthesis of microcrystalline $Cu_3(BTC)_2$ MOF (HKUST-1)[12] and the Ru@HKUST-1 composites (Ru@HKUST-1a, -1b and -1c) with different contents of Ru was achieved by one-pot solvothermal reaction of $Cu(NO_3)_2.3H_2O$ and $RuCl_3.xH_2O$ with BTC in an ethanol and *N,N*-dimethylformamide (DMF) mixture at 85 °C (Fig. 1; Table S1). During the solvothermal process, Ru nanoparticles were uniformly encapsulated into the octahedron-shaped HKUST-1 crystals (vide infra). The pyrolysis of HKUST-1 or Ru@HKUST-1a, -1b and -1c at 800 °C in an argon atmosphere yielded porous carbon with stable and ultrafine Cu or Cu/Ru nanoparticles embedded inside (Cu@C or Cu/Ru@C-1a, -1b and -1c) through a morphology-preserved thermal transformation process,[13] as observed by scanning electron microscopy (SEM) and transmission electron microscopy (TEM) analyses (vide infra) (Fig. 2; Fig. S1-S4).

Experimental

Materials: All the reagents and solvents used for the synthesis were commercially available and used without further purification. Copper (II) nitrate trihydrate ($Cu(NO_3)_2.3H_2O$, Sigma Aldrich, 98%), benzene-1,3,5-tricarboxylic acid (Sigma Aldrich, 98 %), ruthenium(III) chloride *n*-hydrate ($RuCl_3$.xH2O,

---

[a] *National Institute of Advanced Industrial Science and Technology (AIST), Ikeda, Osaka 563-8577, Japan. Fax: +81-72-751-9629; Tel: +81-72-751-9562. *E-mail: q.xu@aist.go.jp*

[b] *Graduate School of Engineering, Kobe University, Nada Ku, Kobe, Hyogo 657-8501, Japan.*

[c] *Toyama National College of Technology, Hongo-machi, Toyama 939-8630, Japan.*

Electronic supplementary information (ESI) available: Materials, instrumentation details, experimental details for the preparation of MOFs, Cu@C, Cu/Ru@C and Ru@(Cu@C) composites, procedures for determination of catalytic activities, additional SEM and TEM images, electron tomographic measurements, X-ray diffraction, XPS, FTIR, TGA and other supporting data can be found in the Electronic Supplementary Information. See DOI: 10.1039/x0xx00000x

View Article Online
DOI: 10.1039/C6TA10748F

Wako Pure Chemical Industries, Ltd., 99%) and ammonia borane (NH_3BH_3, JSC Aviabor, 97%) were used as received.

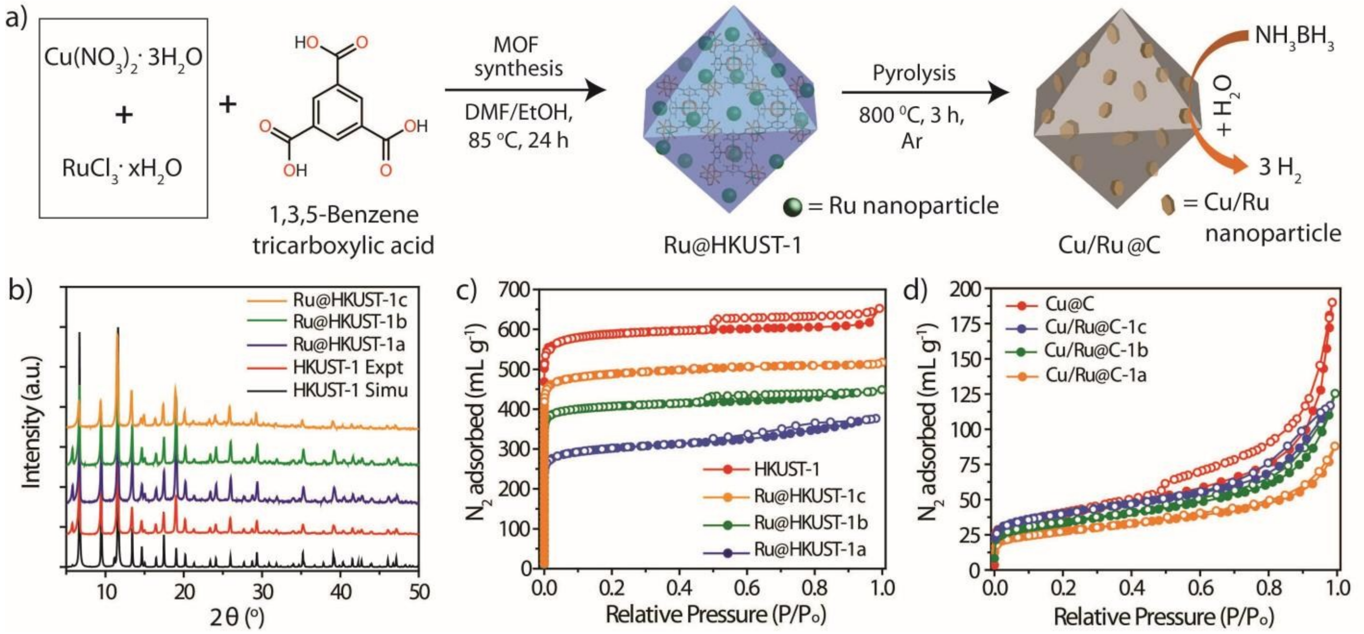

Fig. 1 (a) Schematic illustration of the synthesis of Ru@HKUST and Cu/Ru nanoparticle-embedded porous carbon composites for AB hydrolysis. (b) PXRD patterns of HKUST-1, Ru@HKUST-1a, -1b and -1c, showing the matching profiles with the simulated HKUST-1 pattern. (c) N_2 sorption analyses of HKUST-1, Ru@HKUST-1a, -1b and -1c, showing the decrease in porosity with increasing loading of Ru nanoparticles. (d) N_2 sorption analyses of Cu@C, Cu/Ru@C-1a, -1b and -1c, showing the porosities of carbon composites. Closed and open symbols represent the adsorption and desorption branches, respectively.

Synthesis of Cu_3-BTC_2 MOF (HKUST-1): 1.16 g $Cu(NO_3)_2.3H_2O$ (4.84 mmol) was dissolved in 25 mL ethanol at 60 °C. A solution of 0.491 g BTC (2.34 mmol) in 25 mL DMF was added under stirring and the reaction mixture was refluxed for 6 h at 85 °C. Then, the reaction mixture was transferred into a Teflon-lined autoclave and heated at 85 °C for 12 h. After cooling the autoclave to room temperature, the obtained material was filtered and washed with DMF (3 x 25 mL) and ethanol (3 x 25 mL). The sample was dried at 60 °C for 6 h and 150 °C for 18 h under vacuum.

Synthesis of Ru@HKUST: For the synthesis of Ru@HKUST-1a, 0.932 g $Cu(NO_3)_2.3H_2O$ (3.87 mmol) and 0.258 g $RuCl_3.xH_2O$ (0.97 mmol) were dissolved in 25 mL ethanol at 60 °C. A solution of 0.491 g BTC (2.34 mmol) in 25 mL DMF was added under stirring and the reaction mixture was refluxed for 6 h at 85 °C. Then, the reaction mixture was transferred into a Teflon-lined autoclave and heated at 85 °C for 12 h. After cooling the autoclave to room temperature, the obtained material was filtered and washed with DMF (3 x 25 mL) and ethanol (3 x 25 mL). The sample was dried at 60 °C for 6 h and 150 °C for 18 h under vacuum. The syntheses of Ru@HKUST-1b (0.990 g $Cu(NO_3)_2.3H_2O$ (4.11 mmol) and 0.190 g $RuCl_3.xH_2O$ (0.73 mmol)) and Ru@HKUST-1c (1.05 g $Cu(NO_3)_2.3H_2O$ (4.35 mmol) and 0.130 g $RuCl_3.xH_2O$ (0.49 mmol)) were performed by following the same procedure except using the different amounts of metal salts.

Synthesis of carbon composites: The activated sample of HKUST-1, Ru@HKUST-1a, -1b or -1c (0.50 g) was transferred into a ceramic boat and placed into a temperature-programmed furnace. The sample was heated slowly from room temperature to 800 °C in 4 h and then kept at 800 °C for 3 h under flowing argon gas. The furnace was allowed to cool down to room temperature naturally in argon atmosphere. The resultant brown coloured material of Cu@C or Cu/Ru@C in 25-30 % yield was collected directly from the ceramic boat and used without further purification.

Synthesis of Ru@(Cu@C)-3.4 wt.% and Ru@(Cu@C)-9.4 wt.%: In the typical syntheses, 0.100 g of as-synthesized Cu@C was dispersed in 5 mL of water/ethanol (2:1) solvent and the mixture was sonicated for 10 min until it became homogeneous. After stirring for 30 min, $RuCl_3.xH_20$ (6.96 mg for Ru@(Cu@C)-3.4 wt.%; 19.24 mg for Ru@(Cu@C)-9.4 wt.%) dissolved in 2 ml distilled water was added dropwise over a period of 5 min with constant vigorous stirring. The resulting solution was continuously stirred for 60 min. The reduction of Ru^{3+}@(Cu@C) was carried out by adding 5 mL freshly prepared 1 M aqueous $NaBH_4$ solution under vigorous stirring, resulting in the generation of catalysts as a dark brown suspension. The synthesized sample was collected by centrifuging, dried at 100 °C under vacuum, and used for the catalytic reactions.

Catalytic hydrolysis of ammonia borane: The hydrolysis of ammonia borane (NH_3BH_3, AB) can be briefly expressed as the formula:

$$NH_3BH_3 + 4H_2O \rightarrow NH^{4+} + B(OH)^{4-} + 3H_2$$

View Article Online
DOI: 10.1039/C6TA10748F

The activity of catalysts towards the hydrolysis of AB was determined by measuring the rate of hydrogen evolution. The experimental setup for measuring the hydrogen evolution from the aqueous AB solution is the same as previously reported.[10a] In general, a mixture of catalyst (50 mg) and distilled water (3 mL) was placed in a two-necked round-bottomed flask (30 mL), which was placed in a water bath at room temperature under ambient atmosphere. A gas burette filled with water was connected to the reaction flask to measure the volume of hydrogen. The reaction started when aqueous AB solution (1 mmol in 1 mL water) was injected into the mixture using a syringe. The volume of the evolved hydrogen gas was monitored by recording the displacement of water in the gas burette. The reaction was completed when there was no more gas generation.

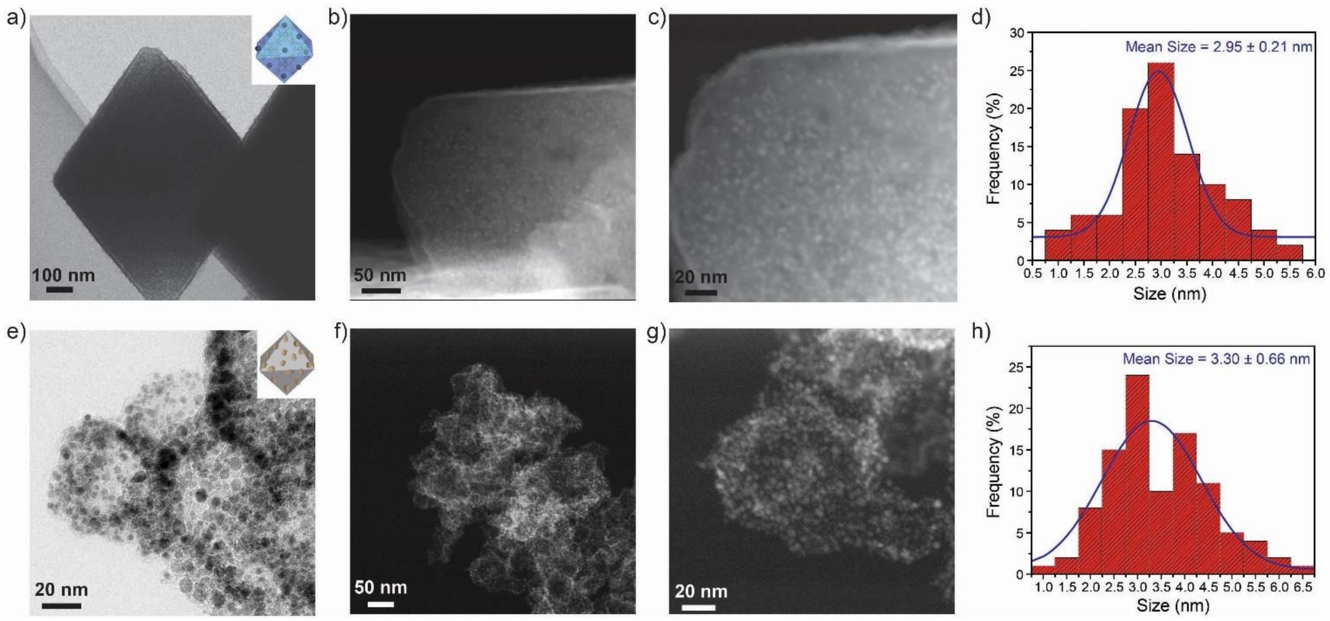

Fig. 2 (a) TEM image of Ru@HKUST-1b, showing the octahedron-shaped morphology of MOF crystals. (b, c) HAADF-STEM images of Ru@HKUST-1b, showing the presence of highly dispersed and ultrafine Ru nanoparticles in the crystal matrix, without aggregation on outer surface. (d) Size histogram of Ru nanoparticles in Ru@HKUST-1b. (e) TEM image of Cu/Ru@C-1b, showing the highly dispersed Cu/Ru nanoparticle-embedded porous carbon composites. (f, g) HAADF-STEM images of Cu/Ru@C-1b, showing the ultrafine Cu/Ru nanoparticle-embedded porous carbon. (h) Size histogram of Cu/Ru nanoparticles in Cu/Ru@C-1b.

Results and discussion

The powder X-ray diffraction (PXRD) profiles of Ru@HKUST-1a, -1b and -1c match well with the corresponding diffractions of HKUST-1 synthesized by the similar method and the simulated PXRD pattern of HKUST-1, indicating the high crystallinity and the same structural integrity of Ru nanoparticle-encapsulated HKUST-1 (Fig. 1b).[12] Moreover, no diffractions were detected for Ru nanoparticles in Ru@HKUST-1a, -1b and -1c, indicating the encapsulation of very small Ru nanoparticles in MOF matrix. Further, the similar coordination environment in HKUST-1, Ru@HKUST-1a, -1b and -1c has been verified using Fourier transform infrared spectroscopy (FTIR) analyses (Fig. S5). The inductively coupled plasma (ICP) analysis for Ru@HKUST-1b confirmed the presence of Cu (21.2 wt.%) and Ru (3.4 wt.%) (Table S1). Thermogravimetric analyses (TGA) of HKUST-1, Ru@HKUST-1a, -1b and -1c in an argon atmosphere showed the thermal stabilities up to 250 °C (Fig. S6).

The PXRD analyses of Cu@C, Cu/Ru@C-1a, -1b and -1c showed sharp peaks at ~44, 51 and 74°, corresponding to the characteristic diffractions of Cu (cubic) (Fig. S7). In addition, the less intense peaks in the PXRD profiles of Cu/Ru@C-1a, -1b and -1c at ~38, 42, 44, 58, 69 and 79° correspond to the characteristic diffractions of Ru (hcp). No additional peaks were observed for metal oxides and other impurities in the carbon matrix, in agreement with the X-ray photoelectron spectroscopic (XPS) analyses (Fig. S8). The XPS investigation of Cu/Ru@C-1b at the Cu 2*p* and Ru 3*d* levels confirmed the presence of metallic Cu and Ru in the carbon matrix. Since Raman I_D/IG ratios (where I_D and I_G are the Raman intensities of D-band and G-band at ~1325 and ~1590 cm^{-1}, respectively) are widely used to evaluate the degree of graphitization of carbon materials,[14] we have performed Raman analyses for the as-synthesized samples of Cu@C, Cu/Ru@C-1a, -1b and -1c. As shown in Fig. S7, the relative intensity (I_D/I_G) ratios for Cu@C, Cu/Ru@C-1a, -1b and -1c are 1.00, 1.04, 0.97 and 0.96, respectively, which suggest the formation of highly graphitic carbon during the pyrolysis of MOFs.[15] With different Cu/Ru ratios in the starting materials of Ru@HKUST composites, the

View Article Online
DOI: 10.1039/C6TA10748F

resulted Cu/Ru@C composites showed different Cu/Ru ratios, as revealed by ICP analyses (Table S2).

The N_2 sorption isotherms of HKUST-1 show a surface area of 1762 m^2g^{-1}, close to the values previously reported (Fig. 1c).[12] As compared with pristine HKUST-1, the decrease in N_2 uptake, Brunauer–Emmett–Teller (BET) surface area and pore volume of the Ru@HKUST-1a, -1b and -1c samples indicates that the cavities of the host frameworks are occupied and/or blocked by the encapsulated Ru nanoparticles in MOF matrix (Fig. 1c, Fig. S3 and S9, Table S1), as observed in the cases of loading metal nanoparticles to MOF-5, ZIF-8 and other porous materials.[8,9,16] As expected, the pore size distributions for HKUST-1, Ru@HKUST-1a, -1b and -1c calculated using non-local density functional theory (NLDFT) method confirm the formation of micropores in MOF matrix (Fig. S9). The N_2 sorption analyses of Cu@C, Cu/Ru@C-1a, -1b and -1c show typical type IV isotherms with the surface areas of 135, 92, 113 and 139 m^2g^{-1}, respectively (Fig. 1d). As calculated from N_2 sorption isotherms, Cu@C, Cu/Ru@C-1a, -1b and -1c show both micro- and meso-pores (Fig. S9).

SEM analyses of HKUST-1, Ru@HKUST-1a, -1b and -1c show the formation of micro-crystalline octahedra (Fig. S1). TEM analyses of Ru@HKUST-1b further confirm their octahedron-shaped morphology (Fig. 2a; Fig. S3). High-resolution TEM (HRTEM) and high-angle annular dark field scanning TEM (HAADF-STEM) images of Ru@HKUST-1b substantiate the encapsulation of Ru nanoparticles of an average size of 2-3 nm inside the MOF matrix (Fig. 2b-2d; Fig. S3). These HRTEM and HAADF-STEM images showed no aggregation of Ru nanoparticles in the interior of MOF matrix as well as on the exterior surface of MOF crystals (Fig. S3).

As observed in SEM analyses, Cu@C, Cu/Ru@C-1a, -1b and -1c preserve the parent MOF precursor morphology through the thermal transformation of MOF to carbon composites (Fig. S2). The TEM images of Cu/Ru@C-1b show the ultrafine Cu/Ru nanoparticle-embedded porous carbon structures (Fig. 2e), suggesting the expediency of octahedron-shaped MOF nanostructures for the fabrication of porous carbon composites through the morphology-preserved thermal transformation of MOF precursor,[13,17] without using polymer and other templates to control the damage of MOF morphology.[18] The HRTEM and HAADF-STEM images of Cu/Ru@C-1b illustrate the formation of tiny Cu/Ru nanoparticle (3-4 nm) embedded porous carbon structures (Fig. 2f-2h; Fig. S4). Additionally, the electron tomographic measurements demonstrate the uniform 3D distribution of the Cu/Ru nanoparticles throughout the carbon octahedron (Movie S1). It is reasonable to consider that during the prolonged heating (3 h) of Ru@HKUST-1b at 800 °C, the MOF crystallites were converted into carbon, ultrafine Cu/Ru nanoparticles and other volatile products. We believe that during the thermal treatment, highly graphitic carbon around the Cu/Ru nanoparticles depressed the sintering of Cu/Ru nanoparticles, resulting in the fine distribution of tiny nanoparticles in carbon matrix,[19] as observed in the HRTEM images and Raman analysis of Cu/Ru@C-1b (Fig. S4 and S7).

As observed in SEM analyses, Cu@C, Cu/Ru@C-1a, -1b and -1c preserve the parent MOF precursor morphology through the thermal transformation of MOF to carbon composites (Fig. S2). The TEM images of Cu/Ru@C-1b show the ultrafine Cu/Ru nanoparticle-embedded porous carbon structures (Fig. 2e), suggesting the expediency of octahedron-shaped MOF nanostructures for the fabrication of porous carbon composites through the morphology-preserved thermal transformation of MOF precursor,[13,17] without using polymer and other templates to control the damage of MOF morphology.[18] The HRTEM and HAADF-STEM images of Cu/Ru@C-1b illustrate the formation of tiny Cu/Ru nanoparticle (3-4 nm) embedded porous carbon structures (Fig. 2f-2h; Fig. S4). Additionally, the electron tomographic measurements demonstrate the uniform 3D distribution of the Cu/Ru nanoparticles throughout the carbon octahedron (Movie S1). It is reasonable to consider that during the prolonged heating (3 h) of Ru@HKUST-1b at 800 °C, the MOF crystallites were converted into carbon, ultrafine Cu/Ru nanoparticles and other volatile products. We believe that during the thermal treatment, highly graphitic carbon around the Cu/Ru nanoparticles depressed the sintering of Cu/Ru nanoparticles, resulting in the fine distribution of tiny nanoparticles in carbon matrix,[19] as observed in the HRTEM images and Raman analysis of Cu/Ru@C-1b (Fig. S4 and S7).

It is well-known that ammonia borane is a promising material for chemical hydrogen storage, from which hydrogen can be released through hydrolysis.[10,11] We have evaluated the catalytic activity of the Cu/Ru nanoparticle-embedded porous carbon composites for AB hydrolysis. The reaction was initiated by introducing aqueous AB solution into the reaction flask containing the as-synthesized catalysts with vigorous shaking at room temperature. H_2 generated from the AB hydrolysis was collected in the burette, with which the H_2 volume was monitored. Fig. 3a shows the H_2 generation using carbon composites Cu@C, Cu/Ru@C-1a, -1b and -1c with different loadings of Cu and/or Cu/Ru (Table S2). It is revealed that Cu/Ru@C-1b is the most active for AB hydrolysis compared to their counterparts, probably due to the fine distribution of Cu/Ru nanoparticles in the porous carbon composite (Table S2). Interestingly, in the case of Cu/Ru@C-1b catalyst, AB hydrolysis reaction is completed in 100 s (Ru/AB = 0.0465 in molar ratio) with a 72 mL H_2 release, corresponding to H_2/AB = 3, giving a turnover frequency (TOF) as high as 97 $\mathrm{molH_2 \cdot molcat^{-1} \cdot min^{-1}}$ based on the amount of Ru (Fig. 3a). Further, the increased H_2 release rates from the AB hydrolysis have been observed at elevated temperatures (Fig. 3b). The apparent activation energy (E_a) of this reaction over Cu/Ru@C-1b was estimated to be 39.2 kJ mol^{-1} within the temperature range of 293–323 K (Fig. S10). On the contrary, the Cu/Ru@C-1a and Cu/Ru@C-1c catalysts synthesized using a similar procedure, but having different Ru contents, show sluggish kinetics and lower TOFs for AB hydrolysis (Fig. 3a; Table S2).

It is found that the productivity of H_2 over the Cu/Ru@C-1b catalyst almost remains unchanged for five runs, which can be attributed to the high stability and durability of metal nanoparticle-embedded porous carbon (Fig. S14). The recyclability of Cu/Ru@C-1b has been analysed by isolating the catalyst after each successive cycle, and the catalytic activity remained almost unchanged over 4 cycles, suggesting the

View Article Online
DOI: 10.1039/C6TA10748F

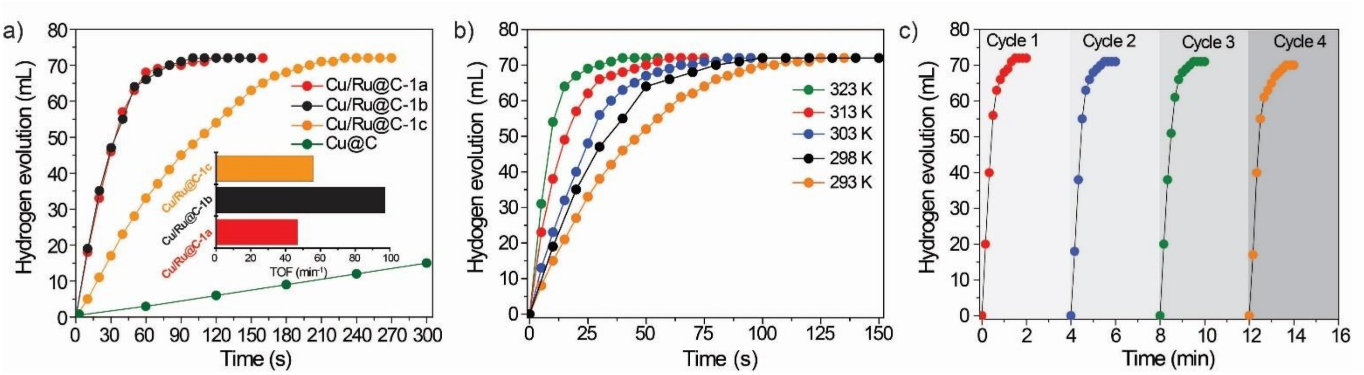

Fig. 3 a) Plots of time *vs.* volume of hydrogen generated from hydrolysis of AB (1 mmol) at 298 K catalyzed by the Cu@C, Cu/Ru@C-1a, -1b and -1c catalysts (50 mg). Inset: the corresponding TOF values on the basis of Ru in the catalysts. b) Temperature dependent catalytic activity of Cu/Ru@C-1b for AB hydrolysis. c) Recyclability test for the hydrogen generation from aqueous AB solution catalyzed by isolated Cu/Ru@C-1b after each successive cycle, showing almost unchanged catalytic activity over 4 cycles.

Table 1. Comparative TOF and energy of activation observed for CuRu@C-2 with literature reported materials.

Catalyst	**TOF ($molH_2.mol_{cat.}$ min^{-1})**	**Energy of activation ($kJ\ mol^{-1}$)**	**Reference**
RGO/Pd	6	51	22a
Pd/zeolite	6.2	55.9 ± 2.2	22b
Ru/γ-Al_2O_3	23	67.0	22c
Ru@Al_2O_3	39.6	46 ± 2	22d
Pd@MIL-101	45	-	22e
Ru(0) nano-clusters	75	47 ± 2.2	22f
Ru/graphene	100	11.7	20c
Ru(0)@X–NW	135	77	22g
Ru(0)/HAp	137	58 ± 2	22h
Ru@MIL-101	187	-	22i
Ru@MIL-53(Cr)	260.8	28.9	22j
Ru@MIL-53(Al)	266.9	33.7	22j
Ru(0)@MWCNT	329	33 ± 2	22k
Ru/C	429.5	34.81 ± 0.12	22l
Pt@MIL-101 (Cr)	446.4	-	8a
Ru/graphene	600	12.7	20h
Pt/CNTs-O-HT	567	-	22m
Rh^0/CeO_2	1350	43 ± 2	22n
MCM-1@$Cu_{0.2}Ni_{0.8}$	10.7	38	23a
RuCu/γ-Al_2O_3	33.0	52.0	23b
RuCo/γ-Al_2O_3	66.3	47.0	23b
$Co_{35}Pd_{65}$/C	22.7	27.5	11g
AuNi@MIL-101_a	66.2	-	8b
CuRu@C-1b	97	39.2	This work
Ag@Co/graphene	102.4	20.03	23c
$Ru_1Cu_{7.5}$/graphene	135	30.59	21b
NiRu@MIL-101	272	-	23d
Pd@Co/graphene	916	-	23e

durability of catalyst for AB hydrolysis (Fig. 3c). PXRD analyses of Cu/Ru@C-1b after catalysis showed no significant change in the diffraction patterns (Fig. S11). The high activity and good durability of Cu/Ru@C-1b demonstrate the great potential of Cu/Ru nanoparticle-embedded porous carbon composites for AB hydrolysis. In addition, the catalytic activity of Cu/Ru@C-1b is among the highest reported for the monometallic and bimetallic catalysts (Table 1).[10,11,20-23] In a control experiment, the catalysts (Ru@(Cu@C)-3.4 and 9.4 wt.%) prepared by supporting 3.4 and 9.4 wt.% of Ru onto the Cu@C composite using conventional impregnation method showed much lower catalytic activities and durabilities compared to Cu/Ru@C-1b (Fig. S12 and S13), suggesting the importance of the use of *in situ* synthesized Ru nanoparticle-encapsulated MOF (HKUST-1) as the self-dedicated template/precursor for the preparation of metal nanoparticle-embedded porous carbon composites. Also, in additional blank experiment, we have synthesized Cu/Ru nanoparticle-supported carbonaceous material by the direct pyrolysis of the starting materials ($RuCl_3.xH_2O$, $Cu(NO_3)_2.3H_2O$ and BTC linker) at 800 °C under argon atmosphere. The ammonia borane hydrolysis studies carried out using as-synthesized carbonaceous sample showed negligible catalytic activity, signifying the importance of MOF template for the preparation of active catalyst (Fig. S15). As HKUST-1 and Ru@HKUST-1a, -1b and -1c are not stable in aqueous medium, the feasibility of using them as catalysts for the hydrolysis of AB

View Article Online
DOI: 10.1039/C6TA10748F

has been limited, as confirmed by the TEM and PXRD analyses of the catalysts recovered after the first cycle (Fig. S16).

Conclusions

In summary, for the first time, a facile method for the encapsulation of highly dispersed ultrafine Ru nanoparticles in HKUST-1 has been achieved by solvothermal reaction of the precursors. The thermal transformation of Ru nanoparticle-encapsulated HKUST-1 composites under an inert atmosphere yielded the ultrafine Cu/Ru nanoparticle-embedded porous carbon composites, which exhibit extraordinary catalytic activity for ammonia borane hydrolysis with good durability. During the thermal treatment of Ru@HKUST-1 composites, highly graphitic carbon around the Cu/Ru nanoparticles, depressed the sintering of nanoparticles, resulting in the fine distribution of tiny nanoparticles in carbon matrix. The novel synthesis of highly active and stable metal nanoparticle-embedded porous carbon composites from metal nanoparticle-encapsulated MOFs may pave its future applications in catalytic transformation reactions.

Acknowledgements

The authors acknowledge Japan Society for the Promotion of Science (JSPS) for financial support. P. P. thanks JSPS for postdoctoral fellowship.

Notes and references

1. *(a)* B. C. Gates, *Chem. Rev.* 1995, **95**, 511–522; *(b)* R. Bashyam and P. Zelenay, *Nature* 2006, **443**, 63–66; *(c)* Y. Li and G. A. Somorjai, *Nano Lett.* 2010, **10**, 2289–2295; *(d)* A. K. Singh and Q. Xu, *ChemCatChem* 2013, **5**, 652–676; *(e)* F. Zaera, *Chem. Soc. Rev.* 2013, **42**, 2746–2762; *(f)* R. Schlögl, *Angew. Chem., Int. Ed.* 2015, **54**, 3465–3520; *(g)* A. Corma, *Angew. Chem., Int. Ed.* 2016, **55**, 6112–6113.
2. *(a)* P. Wynblatt and N. A. Gjostein, *Prog. Solid State Chem.* 1975, **9**, 21–58; *(b)* M. A. Newton, C. Belver-Coldeira, A. Martínez-Arias and M. Fernández-García, *Nature Mater.* 2007, **6**, 528–532; *(c)* C. T. Campbell, *Acc. Chem. Res.* 2013, **46**, 1712–1719.
3. *(a)* P. Munnik, P. E. de Jongh and K. P. de Jong, *Chem. Rev.* 2015, **115**, 6687–6718; *(b)* M. D. Argyle and C. H. Bartholomew, *Catalysts* 2015, **5**, 145–269; *(c)* M. B. Gawande, A. Goswami, T. Asefa, H. Guo, A. V. Biradar, D.-L. Peng, R. Zboril and R. S. Varma, *Chem. Soc. Rev.* 2015, **44**, 7540–7590; *(d)* Q.-L. Zhu and Q. Xu, *Chem*, 2016, **1**, 220–245.
4. *(a)* P. M. Arnal, M. Comotti and F. Schuth, *Angew. Chem. Int. Ed.* 2006, **45**, 8224–8227; *(b)* A. Cao and G. Veser, *Nature Mater.* 2010, **9**, 75–81; *(c)* J. A. Farmer and C. T. Campbell, *Science* 2010, **329**, 933–936; *(d)* G. Prieto, J. Zečević, H. Friedrich, K. P. de Jong and P. E. de Jongh, *Nature Mater.* 2013, **12**, 34–39; *(e)* B. Li, B. Sun, X. Qian, W. Li, Z. Wu, Z. Sun, M. Qiao, M. Duke and D. Zhao, *J. Am. Chem. Soc.* 2013, **135**, 1181–1184; *(f)* G. Li, H. Kobayashi, J. M. Taylor, R. Ikeda, Y. Kubota, K. Kato, M. Takata, T. Yamamoto, S. Toh, S. Matsumura and H. Kitagawa, *Nat. Mater.* 2014, **13**, 802–806.
5. *(a)* M. Eddaoudi, D. B. Moler, H. Li, B. Chen, T. M. Reineke, M. O'keeffe and O. M. Yaghi, *Acc. Chem. Res.* 2001, **34**, 319–330; *(b)* G. Férey, C. Mellot-Draznieks, C. Serre, F. Millange, J. Dutour, S. Surblé and I. Margiolaki, *Science* 2005, **309**, 2040–2042; *(c)* R. Banerjee, A. Phan, B. Wang, C. Knobler, H. Furukawa, M. O'Keeffe and O. M. Yaghi, *Science*, 2008, **319**, 939–943; *(d)* S. Horike, S. Shimomura and S. Kitagawa, *Nature Chem.* 2009, **1**, 695–704; *(e)* H.-C. Zhou, J. R. Long and O. M. Yaghi, *Chem. Rev.* 2012, **112**, 673-674; *(f)* A. G. Slater and A. I. Cooper, *Science* 2015, **348**, 988; *(g)* Y. Bai, Y. Dou, L.-H. Xie, W. Rutledge, J.-R. Li and H.-C. Zhou, *Chem. Soc. Rev.* 2016, **45**, 2327–2367.
6. *(a)* L. Ma, C. Abney and W. Lin, *Chem. Soc. Rev.* 2009, **38**, 1248–1256; *(b)* J. Lee, O. K. Farha, J. Roberts, K. A. Scheidt, S. T. Nguyen and J. T. Hupp, *Chem. Soc. Rev.* 2009, **38**, 1450–1459; *(c)* A. H. Chughtai, N. Ahmad, H. A. Younus, A. Laypkov and F. Verpoort, *Chem. Soc. Rev.* 2015, **44**, 6804–6849; *(d)* A. J. Howarth, Y. Liu, P. Li, Z. Li, T. C. Wang, J. T. Hupp and O. K. Farha, *Nat. Rev. Mater.* 2016, **1**, 15018.
7. *(a)* A. Corma, H. García and F. X. Llabrés i Xamena, *Chem. Rev.* 2010, **110**, 4606–4655; *(b)* J. Gascon, A. Corma, F. Kapteijn and F. X. Llabrés i Xamena, *ACS Catal.* 2013, **4**, 361–378; *(c)* Q.-L. Zhu and Q. Xu, *Chem. Soc. Rev.* 2014, **43**, 5468–5512; *(d)* C. R. Kim, T. Uemura and S. Kitagawa, *Chem. Soc. Rev.* 2016, **45**, 3828–3845.
8. *(a)* A. Aijaz, A. Karkamkar, Y. J. Choi, N. Tsumori, E. Rönnebro, T. Autrey, H. Shioyama and Q. Xu, *J. Am. Chem. Soc.* 2012, **134**, 13926-13929; *(b)* Q. L. Zhu, J. Li and Q. Xu, *J. Am. Chem. Soc.* 2013, **135**, 10210–10213; *(c)* Q. Yang, Q. Xu, S.-H. Yu and H.-L. Jiang, *Angew. Chem. Int. Ed.* 2016, **55**, 3685–3689.
9. W. Zhang, G. Lu, C. Cui, Y. Liu, S. Li, W. Yan, C. Xing, Y. R. Chi, Y. Yang and F. Huo, *Adv. Mater.* 2014, **26**, 4056-4060.
10. *(a)* M. Chandra and Q. Xu, *J. Power Sources*, 2006, **156**, 190-194; *(b)* U. Sanyal, U. B. Demirci, B. R. Jagirdar and P. Miele, *ChemSusChem* 2011, **4**, 1731–1739; *(c)* M. Yadav and Q. Xu, *Energy Environ. Sci.* 2012, **5**, 9698–9725; *(d)* A. Rossin and M. Peruzzini, *Chem. Rev.* 2016, **116**, 8848–8872; *(e)* W.-W. Zhan, Q.-L. Zhu and Q. Xu, *ACS Catal.* 2016, **6**, 6892–6905.
11. *(a)* A. Gutowska, L. Li, Y. Shin, C. M. Wang, X. S. Li, J. C. Linehan, R. S. Smith, B. D. Kay, B. Schmid, W. Shaw, M. Gutowski and T. Autrey, *Angew. Chem. Int. Ed.* 2005, **44**, 3578–3582; *(b)* R. J. Keaton, J. M. Blacquiere and R. T. Baker, *J. Am. Chem. Soc.* 2007, **129**, 1844–1845; *(c)* J.-M. Yan, X.-B. Zhang, S. Han, H. Shioyama and Q. Xu, *Angew. Chem. Int. Ed.* 2008, **47**, 2287–2289; *(d)* S.-K. Kim, W.-S. Han, T.-J. Kim, T.-Y. Kim, S. W. Nam, M. Mitoraj, L. Piekos, A. Michalak, S. J. Hwang and S. O. Kang, *J. Am. Chem. Soc.* 2010, **132**, 9954–9955; *(e)* Ö. Metin, V. Mazumder, S. Özkar and S. H. Sun, *J. Am. Chem. Soc.* 2010, **132**, 1468–1469; *(f)* J.-M. Yan, X.-B. Zhang, T. Akita, M. Haruta and Q. Xu, *J. Am. Chem. Soc.* 2010, **132**, 5326–5327; *(g)* D. Sun, V. Mazumder, Ö. Metin and S. Sun, *ACS Nano.* 2011, **5**, 6458–6464; *(h)* P. Z. Li, A. Aijaz and Q. Xu, *Angew. Chem. Int. Ed.* 2012, **51**, 6753–6756; *(i)* C.-Y. Peng, L. Kang, S. Cao, Y. Chen, Z.-S. Lin and W.-F. Fu, *Angew. Chem. Int. Ed.* 2015, **54**, 15725–15729.
12. *(a)* S. S.-Y. Chui, S. M.-F. Lo, J. P. H. A. Charmant, G. A. Orpen and I. D. Williams, *Science* 1999, **283**, 1148–1150; *(b)* L. H. Wee, M. R. Lohe, N. Janssens, S. Kaskel and J. A. Martens, *J. Mater. Chem.* 2012, **22**, 13742–13746; *(c)* O. Kozachuk, I. Luz, F. X. Llabres i Xamena, H. Noei, M. Kauer, H. B. Albada, E. D. Bloch, B. Marler, Y. Wang, M. Muhler and R. A. Fischer, *Angew. Chem. Int. Ed.* 2014, **53**, 7058–7062; *(d)* M. A. Gotthardt, R. Schoch, S. Wolf, M. Bauer and W. Kleist, *Dalton Trans.* 2015, **44**, 2052–2056.
13. *(a)* B. Liu, H. Shioyama, T. Akita and Q. Xu, *J. Am. Chem. Soc.* 2008, **130**, 5390–5391; *(b)* H. L. Jiang, B. Liu, Y. Q. Lan, K. Kuratani, T. Akita, H. Shioyama, F. Q. Zong and Q. Xu, *J. Am. Chem. Soc.* 2011, **133**, 11854-11857; *(c)* M. Hu, J. Reboul, S. Furukawa, N. L. Torad, Q. Ji, P. Srinivasu, K. Ariga, S. Kitagawa and Y. Yamauchi, *J. Am. Chem. Soc.* 2012, **134**, 2864–2867; *(d)* J.-K. Sun and Q. Xu, *Energy Environ. Sci.* 2014, **7**, 2071–2100; *(e)* J. Tang, R. R. Salunkhe, J. Liu, N. L. Torad, M. Imura, S. Furukawa and Y. Yamauchi, *J. Am. Chem. Soc.* 2015, **137**, 1572–1580; *(f)* G. Hao, G. Mondin, Z. Zheng, T. Biemelt, S.

View Article Online
DOI: 10.1039/C6TA10748F

Klosz, R. Schubel, A. Eychmüller and S. Kaskel, *Angew. Chem., Int. Ed.* 2015, **54**, 1941–1945; *(g)* Q. Lin, X. Bu, A. Kong, C. Mao, X. Zhao, F. Bu and P. Feng, *J. Am. Chem. Soc.* 2015, **137**, 2235–2238; *(h)* K. Shen, X. Chen, J. Chen and Y. Li, *ACS Catal.* 2016, **6**, 5887−5903.

14 *(a)* L. A. Lyon, *Anal. Chem.* 1998, **70**, 341R–361R; *(b)* L. G. Cancado, A. Jorio, E. H. Martins Ferreira, F. Stavale, C. A. Achete, R. B. Capaz, M. V. O. Moutinho, A. Lombardo, T. S. Kulmala and A. C. Ferrari, *Nano Lett.* 2011, **11**, 3190–3196.

15 A. Eckmann, A. Felten, A. Mishchenko, L. Britnell, R. Krupke, K. S. Novoselov and C. Casiraghi, *Nano Lett.* 2012, **12**, 3925–3930.

16 *(a)* M. Meilikhov, K. Yusenko, D. Esken, S. Turner, G. V. Tendeloo and R. A. Fischer, *Eur. J. Inorg. Chem.* 2010, **24**, 3701–3714; *(b)* A. Dhakshinamoorthy and H. Garcia, *Chem. Soc. Rev.* 2012, **41**, 5262–5284.

17 *(a)* X. Xu, R. Cao, S. Jeong and J. Cho, *Nano Lett.* 2012, **12**, 4988–4991; *(b)* P. Pachfule, B. P. Biswal and R. Banerjee, *Chem. Eur. J.* 2012, **18**, 11399–11408; *(c)* A. Aijaz, J.-K. Sun, P. Pachfule, T. Uchida and Q. Xu, *Chem. Commun.* 2015, **51**, 13945-13948; *(d)* B. Xia, Y. Yan, N. Li, H. Wu, X. W. Lou and X. Wang, *Nat. Energy* 2016, **1**, 15006; *(e)* P. Pachfule, D. Shinde, M. Majumder and Q. Xu, *Nature Chem.* 2016, **8**, 718–724.

18 W. Bak, H. S. Kim, H. Chun and W. C. Yoo, *Chem. Commun.* 2015, **51**, 7238–7241.

19 *(a)* X. Liu, X. Cui, Y. Liu and Y. Yin, *Nanoscale* 2015, **7**, 18320–18326; *(b)* T. Yang, H. Ling, J.-F. Lamonier, M. Jaroniec, J. Huang, M. J. Monteiro and J. Liu, *NPG Asia Mater.* 2016, **8**, e240.

20 *(a)* Y. Li, L. Xie, Y. Li, J. Zheng and X. Li, *Chem. Eur. J.* 2009, **15**, 8951–8954; *(b)* M. Zahmakiran, T. Ayvali and K. Philippot, *Langmuir* 2012, **28**, 4908–4914; (c) N. Cao, W. Luo and G. Z. Cheng, *Int. J. Hydrogen Energy* 2013, **38**, 11964–11972; *(d)* E. K. Abo-Hamed, T. Pennycook, Y. Vaynzof, C. Toprakcioglu, A. Koutsioubas and O. A. Scherman, *Small* 2014, **10**, 3145–3152; *(d)* W. Chen, J. Ji, X. Feng, X. Duan, G. Qian, P. Li, X. Zhou, D. Chen and W. Yuan*, J. Am. Chem. Soc.* 2014, **136**, 16736–16739; (*e*) Q. Yao, W. Shi, G. Feng, Z. H. Lu, X. Zhang, D. Tao, D. Kong and X. Chen, *J. Power Sources*, 2014, **257**, 293–299; *(f)* Q. Yao, Z.-H. Lu, Z. Zhang, X. Chen and Y. Lan, *Sci. Rep.*, 2014, **4**, 7597; *(g)* C. Du, Q. Ao, N. Cao, L. Yang, W. Luo and G. Cheng, *Int. J. Hydrogen Energy* 2015, **40**, 6180−6187; *(h)* H. Ma and C. Na, *ACS Catal.* 2015, **5**, 1726–1735.

21 *(a)* L. T. Guo, Y. Y. Cai, J. M. Ge, Y. N. Zhang, L. H. Gong, X. H. Li, K. X. Wang, Q. Z. Ren, J. Su and J. S. Chen, *ACS Catal.* 2015, **5**, 388-392; *(b)* N. Cao, K. Hu, W. Luo and G. Z. Cheng, *J. Alloys Compd.* 2014, **590**, 241–246; *(c)* H. Ye, Q. Wang, M. Catalano, N. Lu, J. Vermeylen, M. J. Kim, Y. Liu, Y. Sun and X. Xia, *Nano Lett.* 2016, **16**, 2812– 2817; *(d)* K. Mori, K. Miyawaki, H. Yamashita, *ACS Catal.* 2016, **6**, 3128−3135.

22 *(a)* P. X. Xi, F. J. Chen, G. Q. Xie, C. Ma, H. Y. Liu, C. W. Shao, J. Wang, Z. H. Xu, X. M. Xu and Z. Z. Zeng, *Nanoscale* 2012, **4**, 5597–5601; *(b)* M. Rakap and S. Özkar, *Int. J. Hydrogen Energy*, 2010, **35**, 1305–1312; *(c)* G. P. Rachiero, U. B. Demirci and P. Miele, *Catal. Today* 2011, **170**, 85–92; *(d)* H. Can and Ö. Metin, *Appl. Catal., B,* 2012, **125**, 304-310; *(e)* H. Dai, J. Su, K. Hu, W. Luo and G. Cheng, *Int. J. Hydrogen Energy* 2014, **39**, 4947−4953; *(f)* F. Durap, M. Zahmakıran and S. Özkar, *Int. J. Hydrogen Energy* 2009, **34**, 7223−7230; *(g)* S. Akbayrak and S. Özkar, *Dalton Trans.*, 2014, **43**, 1797−1805; *(h)* S. Akbayrak, P. Erdek and S. Özkar, *Appl. Catal. B,* 2013, **142-143**, 187–195; *(i)* T. Liu, Q. Wang, B. Yan, M. Zhao, W. Li and H. Bie, *J. Nanomater.* 2015, **2015**, 679526; *(j)* K. Yang, L. Zhou, G. Yu, X. Xiong, M. Ye, Y. Li, D. Lu, Y. Pan, M. Chen, L. Zhang, D. Gao, Z. Wang, H. Liu and Q. Xia, *Int. J. Hydrogen Energy* 2016, **41**, 6300–6309; *(k)* S. Akbayrak and S. Özkar, *ACS Appl. Mater. Interfaces*, 2012, **4**, 6302-6310; *(l)* H. Liang, G. Chen, S. Desinan, R. Rosei, F. Rosei and D. Ma, *Int. J. Hydrogen Energy* 2012, **37**, 17921−17927; *(m)* W. Chen, J. Ji, X. Duan, G. Qian, P. Li, X. Zhou, D. Chen and W. Yuan, *Chem. Commun.*, 2014, **50**, 2142–2144; *(n)* S. Akbayrak, Y. Tonbul and S. Özkar, *Appl. Catal., B*, 2016, **198**, 162-170.

23 *(a)* Z. H. Lu, J. Li, G. Feng, Q. Yao, F. Zhang, R. Zhou, D. Tao, X. Chen and Z. Yu, *Int. J. Hydrogen Energy* 2014, **39**, 13389–13395; *(b)* G. P. Rachiero, U. B. Demirci and P. Miele, *Int. J. Hydrogen Energy* 2011, **36**, 7051−7065; *(c)* L. Yang, W. Luo and G. Z. Cheng, *ACS Appl. Mater. Interfaces* 2013, **5**, 8231–8240; *(d)* S. Roy, P. Pachfule and Q. Xu, *Eur. J. Inorg. Chem.* 2016, 4353–4357; *(e)* J. Wang, Y. Qin, X. Liu and X. Zhang, *J. Mater. Chem.*, 2012, **22**, 12468–12470.

View Article Online
DOI: 10.1039/C6TA10748F

Journal of Materials Chemistry A

From Ru nanoparticle-encapsulated metal-organic framework to highly catalytically active Cu/Ru nanoparticle-embedded porous carbon

Graphical abstract

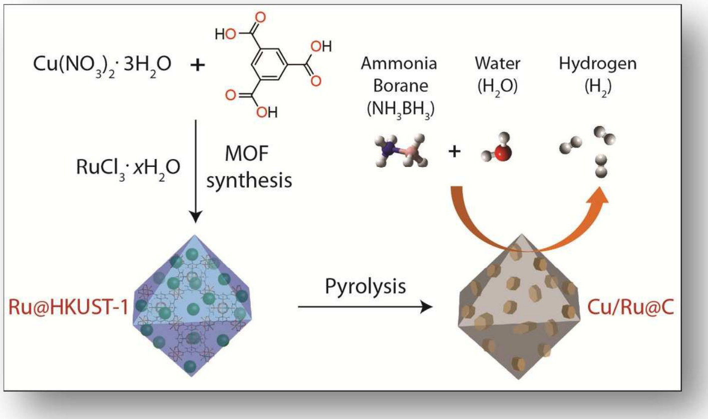

High–temperature pyrolysis of Ru nanoparticle-encapsulated MOF (Ru@HKUST-1) afforded the ultrafine Cu/Ru nanoparticle-embedded porous carbon composites (Cu/Ru@C), which show a high catalytic activity for ammonia borane hydrolysis.